Diagnosis of dynamic cable water barrier using a model-based approach: preliminary studies

Abdelghani Matine[2], Emmanuel Schaeffer[2] and Charles-Henri Bonnard[1,2]
[1] Dpt of Mechatronics, SATIE Lab., École Normale Supérieure de Rennes, Campus de Ker lann, 35170 Bruz, France
[2] Dpt of Electrical Engineering, IREENA Lab., University of Nantes, 37 Boulevard de l'Université BP 406, 44602 Saint-Nazaire

Abstract – Marine renewable energies offer significant potential for decarbonized electric power generation, especially offshore floating wind turbines that take advantage of the stronger and steadier wind blowing far shore. Such farms use dynamic power cables for connecting the floating wind turbines to their seabed power network. These so-called "umbilicals" are continuously subjected to bending and twisting forces. They withstand coupled electrical, thermal and mechanical constraints that may weaken the water barrier, leading potentially in the more or less long term to the destruction of the power cable insulation system, mainly due to the well-known water-treeing phenomena. This justifies the use of cost-effective monitoring systems able to detect any cable insulation problems as soon as possible. Using a model-based approach, we explore the feasibility of exploiting the power cable screen-to-armor capacitances as moisture sensor. The proposed method is based on the online identification of RLC transmission line model structures of the power cable excited by a high voltage pulse generator designed with the latest gallium nitride (GaN) technology. According to the findings of this preliminary parameter sensitivity analysis, it should be possible to detect and locate a water barrier rupture at a very early stage with a spatial resolution of at least 1 meter.

Submarine power cable, Dynamic cable, Water sealing barrier, Predictive maintenance, Diagnosis, Model-based approach, Monitoring, Transmission Line Model, Sensitivity functions.

1. INTRODUCTION

The development of marine renewable energies (MRE) is a key challenge for reducing the current production of greenhouse gases. For this, floating offshore wind turbines are very promising : they take advantage of the stronger and steadier wind blowing far shore and show a far better social acceptability compared to nearshore turbines with jacket or mono-pile fixed foundations. However, they present higher installation and maintenance costs [1, 2, 3, 4, 5], in particular because their maintenance windows are highly dependent on sea-states and weather. In some case, it may be necessary to delay the curative maintenance by several months leading to important operating losses, with a strong impact on the cost of the energy, i.e. with negative consequences on the economical profitability of the MRE farm. Accordingly, it is essential to detect and to locate any defect in the offshore facility as soon as possible, in a cost effective manner and in such a way that it upgrades its predictive maintenance.

Whatever the type of MRE farm (e.g. wind, wave, etc.), one have to install submarine cables which are key elements of the power network and basically of two types : 1) Static cable that is mostly buried in the seabed and transmits power from the farm to the shore has been studied for decades [7, 8, 9], and 2) Dynamic cable that (inter)connects the floating MRE converters to the power hub/substation, for which the MRE industry still has a very little experience feedback [10, 11, 6, 12]. Besides electrical and thermal constraints, the latter must continuously whistand its environmental conditions that impose high dynamic mechanical loads (Fig. 1). Such coupling of stresses can weaken the water barrier, right up to its rupture. The resulting water penetration in the cross-section air gaps may accelerate the oxidation

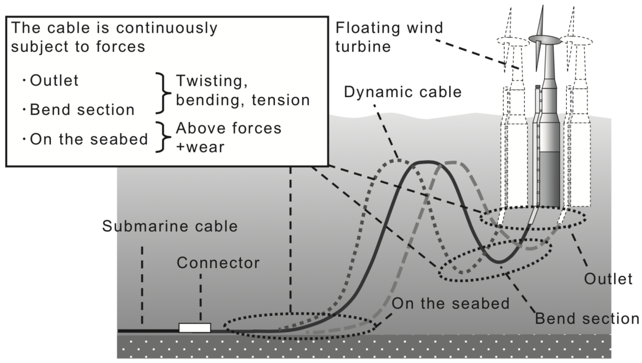

FIG. 1. Dynamic cable connecting the floating wind turbine to the seabed power network [6].

of metallic armor as well as the water-treeing phenomena until the deterioration of the electrical insulation system. For all these reasons, monitoring moisture inside the 300 to 800 meters long dynamic cables has been identified as a key issue for MRE farm predictive maintenance [12, 9, 13, 14, 15]. One might want to use the huge experience of oil & gas industry in terms of design and maintenance of umbilical, but unfortunately it can hardly be applied directly to MRE farms due to the restriction of their economic model that globally needs to lower the overall costs of all their technological bricks [5, 3]. It is therefore essential to propose new monitoring techniques being as cost-effective as possible.

Several approaches can be used to diagnose the insulation system of submarine power cables. One can mention the analysis of partial discharge characteristics [16, 17, 18], the more or less advanced reflectometry techniques used to locate an insulation breakdown [19, 20, 21, 22, 23] or the optical fiber-based techniques [24, 25]. In a previous work [15], we tried to detect a local change of the conductor-to-screen distributed capacitance induced by the growth of a water trees. These trees are mainly induced by moisture [26, 27, 28, 29], so from a predictive maintenance point of view, it appears much more interesting to detect the rupture of the external sealing barrier as soon as possible. Indeed, as the water has just penetrated the filler area while the dielectric insulation between each core and its screen is still unaffected, the cable can still be operated normally for a long time, giving the farm operator the opportunity to optimize the planning of its corrective maintenance. Based on this observation, this paper is concerned with the whole dynamic cable and focuses on the rupture of the first water barrier, i.e. the thin layer that is just below the external sheath of the cable, as depicted in Fig. 3. The resulting water penetration has obviously no physical effect on the resistances and mutual inductances of conductive materials (i.e. armor, screens and phase conductors). Moisture can only leads to a change of the local conductances (of the insulation system, or more generally of the material between two conductive elements) and of the local capacitances between the phase conductors and their surrounding screen or also between screens. In other words, such capacitances represent a distributed sensor that could help us to identify and locate a water barrier defect in addition to other methods.

For this preliminary sensitivity analysis, the temporal response of the dynamic cable subjected to high-frequency high-voltage pulses is simulated by a multi-wire transmission line whose distributed parameter values are obtained by the finite element method (FEM). Then, these synthetic signals are used to evaluate the possibility of detecting a small relative change of the distributed capacitance somewhere along the power cable. The following section presents the proposed model-based diagnosis approach and details the modeling of the cable connected to the pulse generator at one extremity between three paralleled screens and armor. Section 3 details the case study and comments the first results.

2. DIAGNOSIS OF THE DYNAMIC CABLE BY THE MODEL-BASED APPROACH

2.1. *System modeling by continuous-time state-space representation*

Diagnosis of system faults can be addressed by data-driven or model-based approaches, each of them having their own advantages and limitations [30, 31]. Data-driven methods (big data, neuronal network, IA, etc.) are especially interesting when one has a very large amount of data, which is obviously not the case for power umbilicals. We have focused on the model-based approach, using a continuous-time output-error algorithm for system identification [32, 33]. Continuous-time modeling and analysis have many interesting features. In particular, the model parameters are directly related to the system physical characteristics. The diagnosis and prognosis of the system can then be performed by comparing the in-situ estimated parameter values with those given by aging laws, that can be obtained beforehand in laboratories under well-controlled conditions. Concretely, as far as this study is concerned, the challenge consists in finding a model structure (i.e. a set of mathematical equations) for which the time evolution of one or several capacitance estimated values allows to pinpoint a local sealing defect and to relate this change with the moisture content of the concerned cross section. Such structure is generally referred by :

$$M(\boldsymbol{\theta}) \left\{ \begin{array}{l} \dot{\boldsymbol{x}}(t,\boldsymbol{\theta}) = \boldsymbol{f}(\boldsymbol{x}(t,\boldsymbol{\theta}),\boldsymbol{\theta},\boldsymbol{u}(t)) \\ \boldsymbol{y}(t,\boldsymbol{\theta}) = \boldsymbol{g}(\boldsymbol{x}(t,\boldsymbol{\theta}),\boldsymbol{\theta},\boldsymbol{u}(t)) \end{array} \right. \quad (1)$$

where bold and calligraphic letters deal respectively with vectors and matrices, $\boldsymbol{\theta}$ is the unknown parameters, $\boldsymbol{x}$ contains the internal states that physically deals with the energy tanks of the system and $\boldsymbol{u}, \boldsymbol{y}$ are the model input and output that can be scalars or vectors.

2.2. *System identification : some reminders*

The monitored physical parameters of the dynamic cable are estimated using an output error method (OEM) [34] of which principle is summarized in Fig. 2. The identification issue lies in the minimization of the so-called *model-system* distance $D(\theta)$ calculated using the same input during an observation horizon $[t_1 – t_N]$:

$$\theta_{opt} = \arg\min_{\theta} D(\boldsymbol{\theta}) \,, \quad (2)$$

$$D(\boldsymbol{\theta}) = \frac{1}{N.s} \sum_{n=1}^{N} \boldsymbol{e}_n(\boldsymbol{\theta})^t.\mathcal{W}_n^{-1}.\boldsymbol{e}_n(\boldsymbol{\theta}) \,, \quad (3)$$

where N is the number of sample data, s is the number of model outputs, $\boldsymbol{e}_n(\boldsymbol{\theta}) = \boldsymbol{y}_s(t_n) - \boldsymbol{y_m}(t_n,\boldsymbol{\theta})$ is the output error at sample time t_n and $\mathcal{W}_n = \text{diag}\left(\text{Var}(\boldsymbol{y}_m)\right)$ is a diagonal

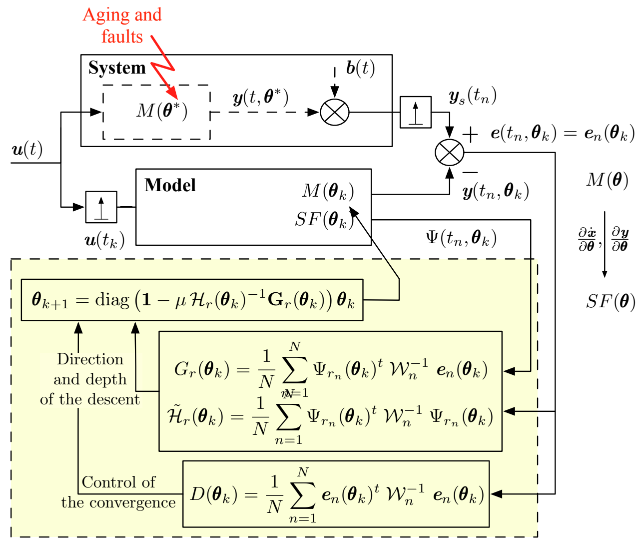

FIG. 2. Principle of the output error method for an output error continuous-time model [32].

weighting matrix required for a-dimensioning the model-system distance. The model outputs being non linear with respect to the model parameters, the minimization of $D(\boldsymbol{\theta})$ is performed by non-linear programming techniques, typically the iterative Levenberg-Marquart algorithm that converges near the optimum to the quasi-newton scheme :

$$\boldsymbol{\theta}_{k+1} = \boldsymbol{\theta}_k - \mu \mathcal{H}_r^{-1}(\boldsymbol{\theta}_k).\boldsymbol{G}_r(\boldsymbol{\theta}_k) \quad (4)$$

where $0 \leq \mu \leq 1$ is used to control the convergence of the kth optimization iteration and $\mathcal{H}_r(\boldsymbol{\theta}_k)$, $\boldsymbol{G}_r(\boldsymbol{\theta}_k)$ are the hessian and the gradient of $D(\boldsymbol{\theta})$ for the current parameter vector $\boldsymbol{\theta}_k$, respectively. Fig. 2 explicits their expressions in relation to uniquely the output error and the relative sensitivity functions $\Psi_r(\boldsymbol{t},\boldsymbol{\theta}) = \text{diag}(\boldsymbol{\theta})\,\Psi(\boldsymbol{t},\boldsymbol{\theta})$, which numerical values at sample times t_n are obtained by the numerical integration of the following matrix state-space representation (derived from the analytical derivation of $M(\boldsymbol{\theta})$ in relation to $\boldsymbol{\theta}$) :

$$SF(\boldsymbol{\theta}) : \left\{ \begin{array}{l} \dot{\Phi}(t,\boldsymbol{\theta}) = \mathcal{F}_{\boldsymbol{x}}(\boldsymbol{x},\boldsymbol{\theta},\boldsymbol{u})\;\Phi(t,\boldsymbol{\theta}) + \mathcal{F}_{\boldsymbol{\theta}}(\boldsymbol{x},\boldsymbol{\theta},\boldsymbol{u}) \\ \Psi(t,\boldsymbol{\theta}) = \mathcal{G}_{\boldsymbol{x}}(\boldsymbol{x},\boldsymbol{\theta},\boldsymbol{u})\;\Phi(t,\boldsymbol{\theta}) + \mathcal{G}_{\boldsymbol{\theta}}(\boldsymbol{x},\boldsymbol{\theta},\boldsymbol{u}) \end{array} \right. \quad (5)$$

where $\mathcal{F}_{\boldsymbol{x}} = [\partial f_i/\partial x_j]$, $\mathcal{G}_{\boldsymbol{x}} = [\partial g_i/\partial x_j]$, $\mathcal{F}_{\boldsymbol{\theta}} = [\partial f_i/\partial \theta_j]$, $\mathcal{G}_{\boldsymbol{\theta}} = [\partial g_i/\partial \theta_j]$ denote the jacobian matrices of $\boldsymbol{f}$ and $\boldsymbol{g}$ in relation to the vectors $\boldsymbol{x}$ and $\boldsymbol{\theta}$, respectively. The requirement of the jacobian analytical expressions and the simulation of both $M(\boldsymbol{\theta})$ and $SF(\boldsymbol{\theta})$ at each iteration of the recurrence (4) is one of the main drawbacks of this output error algotithm. By way of compensation, it does not require any assumption with regard to the noise characteristics and is less sensitive to the modeling noise [35], which in practice is often much higher than the measuring noise, with thus an overriding effect on the model output. Another classic criticism of the OEM is the need to initialize (4) closed to the global optimum. For what concerns the study, it is not a problem for at least two reasons : firstly because cable electrical parameters (such as screen-screen distributed capacitances and inductances) can be easily pre-determined by Finite Element Method (FEM) as briefly reminded in section 3.4, and secondly because the monitored phenomena (evolution of moisture content, water treeing, etc.) show very slow dynamics - and consequently two following sets of parameter estimates remain very closed even if obtained several days or months apart.

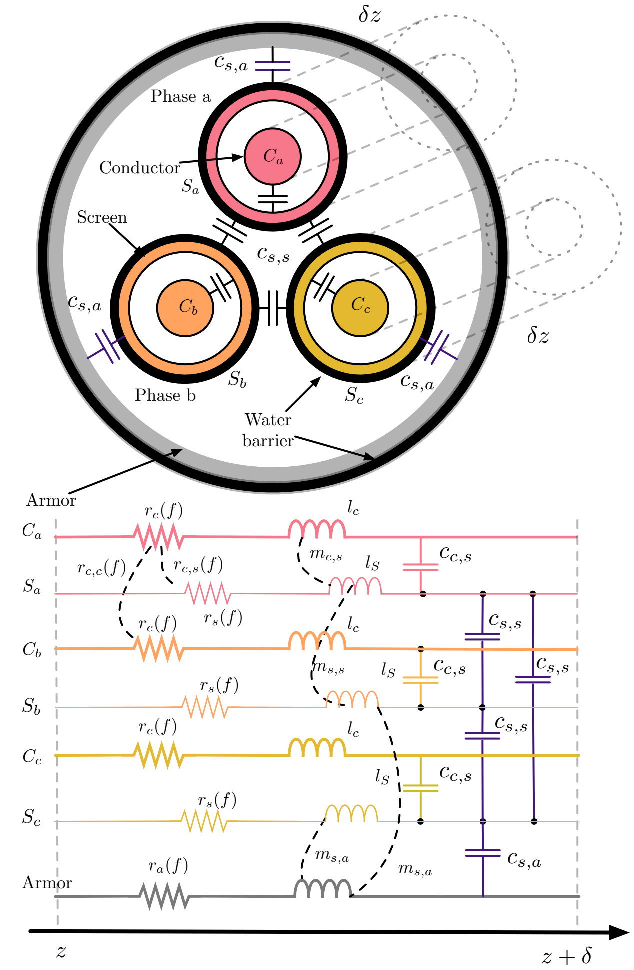

FIG. 3. Definition of the distributed resistances, capacitors and inductances involved in the cable modeling by multi-wire transmission lines.

2.3. *Power cable modeling*

2.3.1. *Simplifying assumptions*

The 3-phase power cable is spatially discretized into N_c elementary cells composed of distributed self and mutual resistors, capacitors and inductance, as depicted in Fig. 3. The unusual mutual terms $r_{c,s}$, $r_{c,a}$ and $r_{s,a}$ deal with the proximity effect between conductors, screens and armor. All self and mutual resistances are highly frequency-dependent (due to skin and proximity effects) and also temperature-dependent. Self and mutual inductances are clearly independent of moisture and depend in a very small extend on the frequency and on the temperature. In a first approach we can then consider them as constant in the whole cable. The capacitances mostly depend on moisture, water trees and other insulation aging that gradually modify the permittivity of the cross-section materials present between two terminals of the capacitor under consideration.

The analytical time differential equations explaining the voltage wave propagation in the power cable depends on how the pulse generator is physically connected to the cable : between a phase conductor and its screen ; between two screens ; between a screen and the armor ; and so on. Many combinations are possible but, depending on the choice, writing the analytical equations can remain quite simple or can become very complex. In this study, we consider the application of the voltage pulses between the three screens connected together (they are thus at the same potential) and the external metallic armor. Physical considerations show that under these simplifying experi-

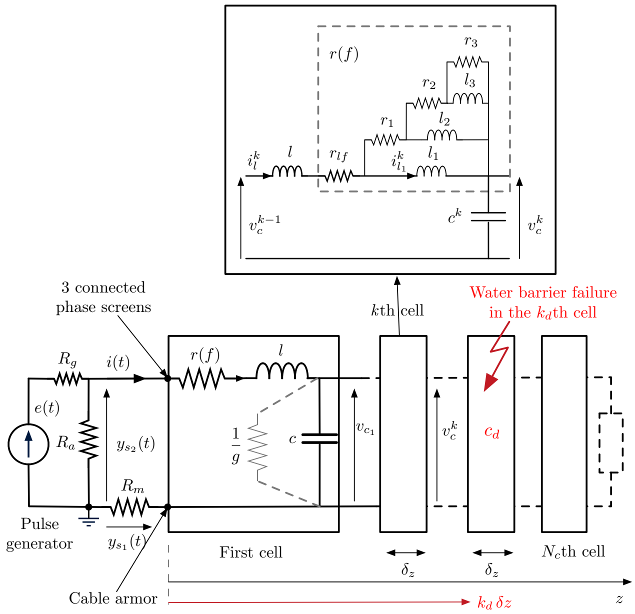

FIG. 4. Electrical model of the whole system (pulse generator and power cable) that must be considered for the simulation of the cable behavior. A water barrier failure results in the variation of the distributed capacitance c of the faulty cell.

mental conditions, not only does the electromagnetic field exhibit a radial symmetry as depicted below by Figs. 7 and 8, but also the propagation of the voltage/current waves in the cable only charges and discharges the three $c_{s,a}$ screen-armor capacitors. Consequently, the problem can be highly simplified down to the study of a conventional two-wires transmission line, as depicted by Fig. 4. This figure presents all subsystems that must be taken into account for the simulation of voltage/current wave propagation in the power cable subjected to voltage pulses.

2.3.2. *Transmission line parameters*

For sake of simplicity, we consider in the following that the electrical parameters of the transmission line (TL) cells do not depend on the position of the cell in the line, except for the capacitance c_d of a faulty cell (see Fig. 4). So, for what concerns the electrical circuit modeling of each cell, one can say that :

— $r(f)$ deals with the distributed resistance of the armor in series with those of the three paralleled screens. And at low frequency, its value r_{lf} is given by :

$$r_{lf} = r_a(0) + r_s(0)/3 \tag{6}$$

where the armor and screen distributed resistances $r_a(f)$ and $r_s(f)$ are defined by Fig. 3.

— c deals with the three distributed screen-armor mutual capacitances $c_{s,a}$ in parallel and thus :

$$c = 3\,c_{s,a} \tag{7}$$

— l physically deals with the magnetic energy stored in a cross-section when a current $i(z,t)$ flows forward in the three paralleled screens and backward in the armor. Using Eq. 25, l can be related to the distributed self and mutual inductances defined by Fig. 3 as follows :

$$l = l_a + \frac{1}{3}l_s + \frac{2}{3}m_{s,s} + 2m_{s,a} \tag{8}$$

where l_a, l_s, $m_{s,a}$ and $m_{s,s}$ are the armor self inductance, the screen self inductance, the screen-armor mutual inductance and the screen-screen mutual inductance, respectively.

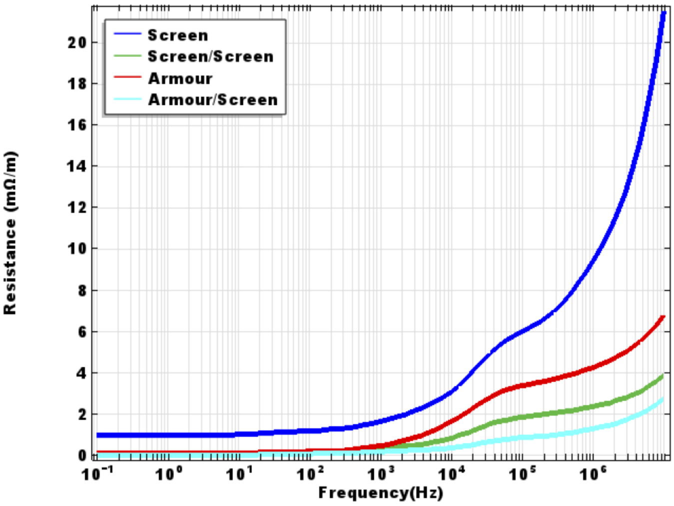

FIG. 5. Evolution of the resistance of the cable conductive components in relation to the frequency obtained by FEM (Comsol) : — $r_s(f)$, — $r_a(f)$, — $r_{s,s}(f)$, — $r_{s,s}(f)$

— the distributed conductance g is not taken into account in an healthy cell because its value is far too small to be sensitized by the excitation protocol.

Moreover, a RL-network of p-stages is classically used to take the proximity and skin effects into account [36] as proposed inside the dotted rectangle in Fig. 4. This requires to introduce the r_p, l_p elements of each p-stage. In order to limit the number of unknown parameters to be estimated, we have studied the frequency and temperature dependence of the resistive and inductive parameters by a finite element method, with the Comsol software [37, 38]. Section 3.4 briefly remind how the numerical values of resistance, capacitance and inductance can be derived from the determination of the electromagnetic field in the cable cross section. Fig. 5 shows the evolution of the self and mutual resistances in the range $[0, 10\,\mathrm{MHz}]$. Using these results, we have shown in [15] that a 4-stages network allows to accurately model the frequency-dependence of the phase conductors, armor and screens. This study also highlighted that the ratios $\alpha_p = r_p/r_{lf}$ and $\beta_p = l_p/l$ are more or less independent of temperature. Consequently, the model of a healthy cable having an unknown homogenous temperature can be parametrized by only the 3 parameters r_{lf}, l, c, the number of cells N_c being chosen high enough to accurately simulate the forward/reverse wave propagation.

2.3.3. State-space model

Let us note $i^k_{r_p}$ and $i^k_{l_p}$ the current flowing respectively in the pth resistor r_p and inductance l_p of the kth cell. We obtain, for a 3-stage network, the following set of equations :

$$\frac{dv_c^k}{dt} = \frac{1}{c^k}(i_l^k - i_l^{k+1}) \tag{9}$$

$$\frac{di^k_{l_3}}{dt} = \frac{r_3}{l_3}\underbrace{(i_l^k - i^k_{l_1} - i^k_{l_2} - i^k_{l_3})}_{i^k_{r_3}} \tag{10}$$

$$\frac{di^k_{l_2}}{dt} = \frac{r_2}{l_2}\underbrace{(i_l^k - i^k_{l_1} - i^k_{l_2})}_{i^k_{r_2}} + \frac{r_3}{l_2} i^k_{r_3} \tag{11}$$

$$\frac{di^k_{l_1}}{dt} = \frac{r_1}{l_1}\underbrace{(i_l^k - i^k_{l_1})}_{i^k_{r_1}} + \frac{r_2}{l_1} i^k_{r_2} + \frac{r_3}{l_1} i^k_{r_3} \tag{12}$$

$$\begin{aligned}\frac{di^k_l}{dt} &= \frac{(v_c^{k-1} - v_c^k)}{l} \\ &\quad - \frac{r_{lf}}{l} i^k_l - \frac{r_1}{l} i^k_{r_1} - \frac{r_2}{l} i^k_{r_2} - \frac{r_3}{l} i^k_{r_3}\end{aligned} \tag{13}$$

that clearly shows the recursive nature of the state variable derivatives. Indeed, reminding that $r_p = \alpha_p\, r_{lf}$ and $l_p = \beta_p\, l$, then a P-stage network is described by :

$$\begin{cases} \frac{d\boldsymbol{i}^k_l}{dt} = \mathcal{A}^k_P \boldsymbol{i}^k_l + \frac{1}{l}(v_c^{k-1} - v_c^k) \\ \frac{dv_c^k}{dt} = \frac{1}{c}(i_l^k - i_l^{k+1}) \end{cases} \tag{14}$$

with $\boldsymbol{i}^k_l = [i^k_l, i^k_{l_1}, \dots, {}^k_{l_P}]^t$ and :

$$\mathcal{A}^k_P = \frac{r_{lf}}{l}\begin{bmatrix} -(1+\sum_{p=1}^{P}\alpha_p) & \sum_{p=1}^{P-1}\alpha_p & \sum_{p=2}^{P-1}\alpha_p & \dots & \alpha_p \\ \sum_{p=1}^{P}\frac{\alpha_p}{\beta_1} & -\sum_{p=1}^{P}\frac{\alpha_p}{\beta_1} & -\sum_{p=2}^{P}\frac{\alpha_p}{\beta_1} & \dots & -\frac{\alpha_P}{\beta_1} \\ \sum_{p=2}^{P}\frac{\alpha_p}{\beta_2} & -\sum_{p=2}^{P}\frac{\alpha_p}{\beta_2} & -\sum_{p=2}^{P}\frac{\alpha_p}{\beta_2} & \dots & -\frac{\alpha_P}{\beta_2} \\ \vdots & \ddots & \ddots & \ddots & \vdots \\ \frac{\alpha_P}{\beta_P} & -\frac{\alpha_P}{\beta_P} & -\frac{\alpha_P}{\beta_P} & \dots & -\frac{\alpha_P}{\beta_P} \end{bmatrix} \tag{15}$$

Then, noting $\boldsymbol{x}^t(t) = [\boldsymbol{i}^1_l(t), \dots, \boldsymbol{i}^{N_c}_l(t), v^1_c(t), \dots, v^{N_c}_c(t)]$ the state-space vector with dimension of $Nc(P+3)$, $\boldsymbol{\theta}^t = [r_{lf}, l, c]$ the parameter vector and $\boldsymbol{y}^t_s(t)$ the voltages measured across the resistances R_a and R_m, one obtains the following state-space representation :

$$M(\boldsymbol{\theta})\begin{cases} \dot{\boldsymbol{x}}(t,\boldsymbol{\theta}) = \mathcal{A}_c(\boldsymbol{\theta})\,\boldsymbol{x}(t,\boldsymbol{\theta}) + \mathcal{B}_c(\boldsymbol{\theta})\,e(t) \\ \boldsymbol{y}(t,\boldsymbol{\theta}) = \mathcal{C}_c\,\boldsymbol{x}(t,\boldsymbol{\theta}) + \mathcal{D}_c\,e(t) \end{cases} \tag{16}$$

with

$$\mathcal{B}^t_c(\boldsymbol{\theta}) = [\frac{R_a}{l(R_a+R_g)}, 0, \dots, 0] \tag{17}$$

$$\mathcal{C}_c = \begin{bmatrix} -\frac{R_a}{(R_a+R_g)} & 0 & \dots & 0 \\ R_m & 0 & \dots & 0 \end{bmatrix} \tag{18}$$

$$\mathcal{D}^t_c = [\frac{R_a}{(R_a+R_g)}, 0] \tag{19}$$

and

$$\mathcal{A}_c(\boldsymbol{\theta}) = \left[\begin{array}{cccc|c} \mathcal{A}^1_P & \mathcal{O} & \dots & \mathcal{O} & \mathcal{L}_P \\ \mathcal{O} & \mathcal{A}^2_P & \ddots & \vdots & \mathcal{L}_P \\ \vdots & \ddots & \ddots & \vdots & \mathcal{L}_P \\ \mathcal{O} & \dots & \dots & \mathcal{A}^{N_c}_P & \mathcal{L}_P \\ \hline \mathcal{C}^1_P & \mathcal{C}^2_P & \dots & \mathcal{C}^{N_c}_P & \mathcal{O}_P \end{array}\right] \tag{20}$$

$$\mathcal{L}_P = \begin{bmatrix} -\frac{1}{l} & 0 & 0 & \dots & 0 \\ \frac{1}{l} & \ddots & \ddots & \ddots & \vdots \\ 0 & \ddots & \ddots & \ddots & \vdots \\ \vdots & \ddots & \ddots & \dots & 0 \\ 0 & \dots & 0 & \frac{1}{l} & -\frac{1}{l} \end{bmatrix} \tag{21}$$

$$\mathcal{C}_P^k = \begin{bmatrix} \frac{1}{c^k} & -\frac{1}{c^k} & 0 & \dots & 0 \\ 0 & \ddots & \ddots & \ddots & \vdots \\ 0 & \ddots & \ddots & \ddots & 0 \\ \vdots & \ddots & \ddots & \dots & -\frac{1}{c^k} \\ 0 & 0 & \dots & 0 & \frac{1}{c^k} \end{bmatrix} \tag{22}$$

where $\mathcal{A}_P^k$ are defined by 15, with just a difference for the first element of $\mathcal{A}_P^1$ that takes into account the connected pulse generator :

$$\mathcal{A}_P^1(1,1) = -\frac{1}{l}\left(R_m + \frac{R_a\,R_g}{R_a\,R_g} + r_{lf}(1 + \sum_{p=1}^{P}\alpha_p)\right) \tag{23}$$

Note that taking the distributed conductance ρ into account uniquely modifies the matrix $\mathcal{O}_P$ and that $\mathcal{A}_P^1(N_c, N_c)$ imust be updated similarly to 23 if the power cable is connected to a load at its right end. Moreover, one can observe that it is very simple to take the water ingress in the kth cell : it is sufficient to change the capacitance value of the $\mathcal{C}_P^k$ matrix.

3. SENSITIVITY ANALYSIS

3.1. Case study description

As said in introduction, this work is the continuation of the study based on the 3-phase, 20 kV, 8 MVA submarine cable of the SEM-REV French multi-technology open sea testing site managed by Ecole Centrale de Nantes. The previous work considered the screen-to-conductor transmission line whereas this study consider the screens-to-armor TL and explores the possibility of locating a fault resulting in the relative variation of the screens-to-armor distributed capacitance c_d (see Fig. 4) at an unknown distance $k\,\delta z$ of the cable extremity, δz being the length of an elementary cell (see. Fig. 4). For this, we use the above state-space model (16) to simulate the cable input-output behavior in presence of a fault in the k_dth cell, where the value of c_d is related to the water content of he concerned "faulty cell". A realistic range of evolution of the distributed capacitance $c_{s,s}$ and $c_{s,a}$ can be obtained by FEM. Fig. 6 shows the evolution of the armor-to-screen and screen-to-screen capacitances in relation to the moisture content inside the cross section, the permittivity of the medium not filled by synthetic filler changing progressively from that of air to that of water.

3.2. Model-System convolution

Then the simulated signals are used to identify a series of faulty-models $M_{k_d}(\boldsymbol{\theta}_d)$, $k_d \in [0\,N_c]$, with $\boldsymbol{\theta}_d^t = [r_{lf}, l, c, c_d]$, c_d being the unknown distributed capacitance of the kth cell supposed to be the faulty one. We can hope that the k_dth model $M_{k_d}(\hat{\boldsymbol{\theta}}_d)$ that presents the lowest error energy deals with the right position of the faulty cell, and that the estimated value $\hat{c}_d$ deals with the right armor-to-screen capacitance of this faulty cell. In other words, we perform a kind of convolution between the model and the system. This approach limits the impact of the modeling noise which remains significant given that the model poorly simulate all very high-frequency phenomena.

Of course, we also consider the measurement noise introduced by the 12 bits ADC (the picoscope 5444D, 1 GS/s, 200 MHz analog bandwidth).

3.3. Considerations of the pulse generator

In order to respect the MRE cost constraints, we have developed a high voltage pulse generator which, combined with a cost-effective 12 bits 1 GS/s datalogger, provides a 2 k€ per cable monitoring system. This pulse generator consists in a 650 V GaN half bridge driven with a 1 ns deadtime to limit the cross-conduction. Thanks to an in depth PCB layout optimization and a very low total gate charge of the latest GaN FETs, we succeeded to apply 400 V square pulses with rise/fall times of less than 8 ns and with very small voltage ripples. For realistic simulations, we therefore consider $e(t)$ as a quasi ideal square signal, with 60 V/ns slewrates but without any voltage ripple. The resistances R_m and R_a have been introduced for the measurement of current and voltage. R_a also plays the role of matching resistance limiting high frequency oscillations and over-voltage that should destroy the pulse generator. R_g deals with the drain-to-source on resistance, its value is less than 100 mΩ.

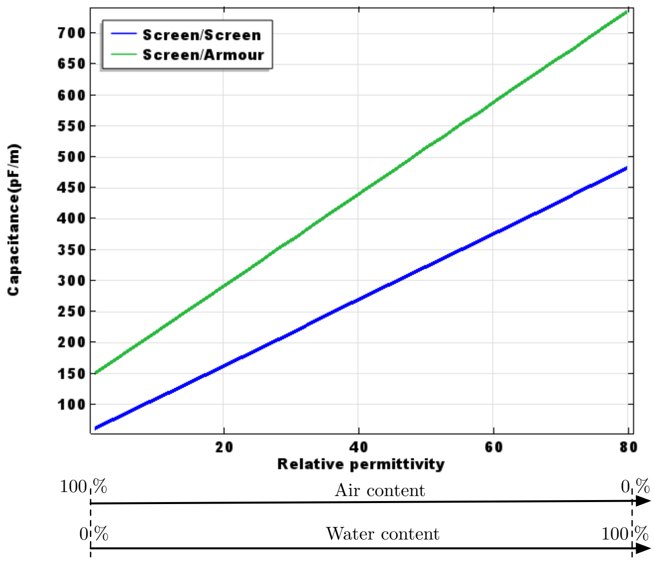

FIG. 6. Evolution of the armor-to-screens capacitance in relation to the moisture content of the medium (inside the cross section), its permittivity changing progressively from that of air to that of water.

3.4. Numerical determination of the distributed parameters by finite element method (Comsol)

The self and mutual capacitances of a set of N conductors can be calculated independently of the frequency using the following expression of the electrostatic energy :

$$W_e = \frac{1}{2}\sum_{i=1}^{N} C_{i,i}V_i^2 - \sum_{i=1}^{N}\left(\sum_{\substack{j=1\\ j\neq i}}^{N} C_{i,j}V_iV_j\right) \tag{24}$$

where $C_{i,i}$ and $C_{i,j}$ are the self and mutual capacitance of the conductors i and j, respectively, and V_i, V_j their electrostatic potential. Then the numerical value of $C_{i,i}$ is obtained by applying $V_i = 1,\ V_{j\neq i} = 0$ and $C_{i,j}$ by applying $V_i = 1,\ V_j = -1$. To illustrate the method, Fig. 7 shows the electric field obtained by applying a $2\,V$ voltage drop between the armor (at potential $+1$ V and the three connected screens at -1 V).

In the same way, the self and mutual resistances and inductances of a set of N conductors can be calculated using the following expression of the magnetic energy and Joule losses :

$$W_m = \frac{1}{2}\sum_{i=1}^{N}\left(\sum_{j=1}^{N} L_{i,j}(f)I_iI_j\right) \tag{25}$$

$$P_j = \sum_{i=1}^{N}\left(\sum_{j=1}^{N} R_{i,j}(f)I_iI_j\right) \tag{26}$$

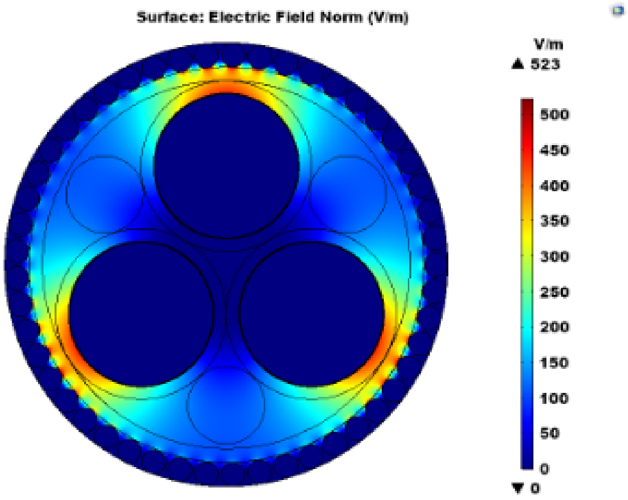

FIG. 7. Computation of the electrostatic field used to post-process the mutual armor-screens capacitance.

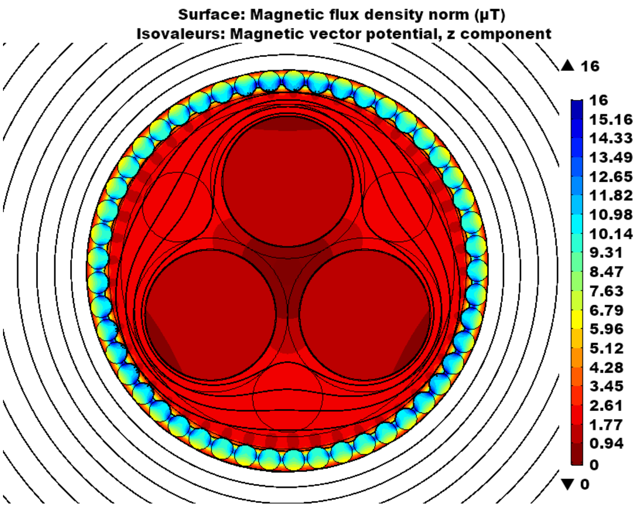

FIG. 8. Computation of the induction field used to post-process the transmission line inductance and resistance.

where $L_{i,i}(f)$, $L_{i,j}(f)$, $R_{i,i}(f)$, $R_{i,j}(f)$, are the self and mutual inductances and resistance of the conductors i and j, respectively, and I_i, I_j the sinusoidal current flowing inside at a given frequency f. For example, Fig. 8 shows the magnetic field density at 100 Hz calculated by FEM for a 1 A current flowing forward in the three paralleled screens and backward in the armor.

3.5. *Considerations of the granularity of the TL model*

Intuitively, the higher the number of cells, the better the model should be able to simulate the healthy cable and the cable with a more or less localized fault. And furthermore, the higher N_c, the more accurately it will be possible to locate precisely a fault in the cable by the model-based approach. In practice, one can observe (see Fig. 9) that the modeling noise firstly decreases significantly and reaches a plate around 240 cells, after which its decrease is compensated by the increase of numerical noise. For the following sensitivity analysis, the input/output behavior of the healthy and faulty cable is therefore simulated with $N_c = 300$, which deals with a good tradeoff between simulation time and spatial granularity. Fig. 10 compares the system outputs measured on the 3-phase, 20 kV, 8 MVA submarine cable of the SEMREV test bench with the ones simulated by

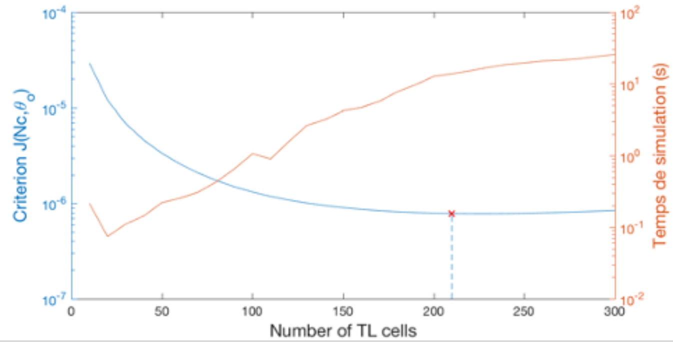

FIG. 9. Evolution of the *Model-System* distance $D(\hat{\boldsymbol{\theta}}_d)$ and the computational cost in relation to the granularity of the transmission line (i.e. the number N_c of cells under consideration) [15].

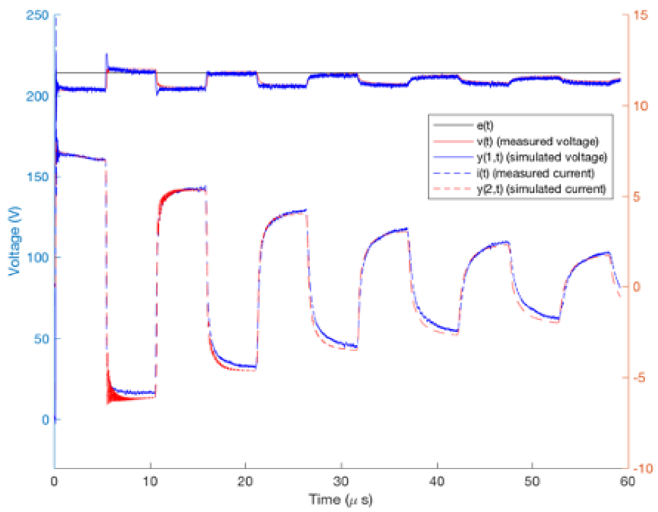

FIG. 10. Comparison between experimental and simulated signals obtained with the 3-phase, 20 kV, 8 MVA submarine cable of the SEMREV test bench and model parameter values calculated par FEM [15].

the model $M(\boldsymbol{\theta})$ for $N_c = 300$ where the numerical values of the distributed parameters r_{lf}, l and c are calculated by FEM as explained in section 3.4. The good agreement between the simulated and measured signals validates the high frequency TL model of the power cable.

3.6. *First results*

Fig. 11 shows the model-system convolution, i.e. the scan of the evolution of the *model-system* normalized distance $D(\hat{\boldsymbol{\theta}}_d)$ in relation to the unknown position of the faulty cell, for different moisture contents in the faulty cell (i.e. for different values of its distributed capacitance), the failure being located within the "simulated" system at 250 m. This figure clearly highlights that the *model-system* convolution should allow to locate a relative evolution of the distributed capacitance greater than 10 %, which must be compared to the evolution of more than 500 % obtained when sea water completely fills the air gaps of the cable cross-section.

4. CONCLUSION

Monitoring the umbilicals of offshore floating wind farms in a cost competitive manner is a key challenge for the development of this renewable energy. In this paper, we explore the diagnosis of the ombilical external sealing barrier by a model-based approach. A sensitivity analysis is performed using the determination of the distributed TL parameters by finite element me-

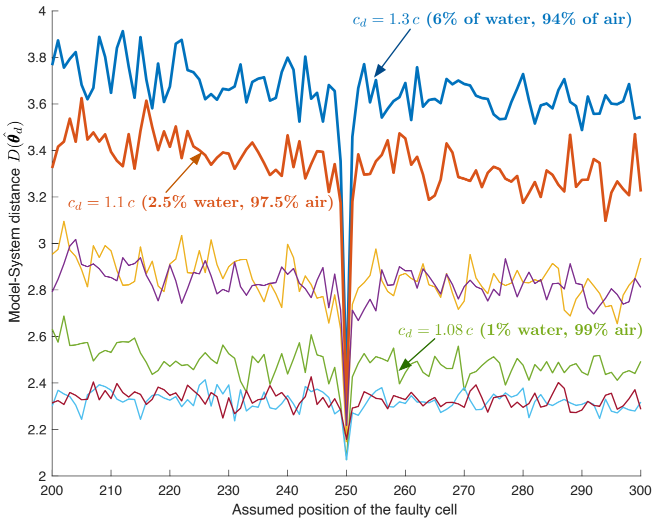

FIG. 11. Evolution of the *Model-Sytem* distance $D(\hat{\boldsymbol{\theta}}_d)$ in relation to the position of the faulty cell, for different water content in the cable cross-section. For example, the upper green line deals with the convolution of the model and the cable of which the water ingress results in an evolution of 30 % of the c_{s_a} distributed capacitance.

thod and an accurate simulation of the power cable. This analysis shows that a water barrier breakdown induced a relative increase of the distributed screen-to-armor capacitance far higher than the threshold value detectable by the identification of a continuous-time state-space model of the dynamic power cable. Next work will compare the sensibility and accuracy of this new approach with the ones of more classical diagnostic methods.

5. ACKNOWLEDGEMENTS

The research work presented in this paper was conducted in the frame of the EMODI project (https ://anr.fr/Projet-ANR-14-CE05-0032) funded by the French National Agency of Research and labelled by the french competitiveness clusters S2E2 (http ://www.s2e2.fr) and EMC2 (http ://www.pole-emc2.fr/), and continued in the frame of the ORIGAMI project, funded by WEAMEC.

6. REFERENCES

[1] C. Kost, S. Shammugam, V. Jülch, H.-T. Nguyen, and T. Schlegl, “Levelized Cost of Electricity- Renewable Energy Technologies,” p. 42.

[2] “Trending Developments in Wind Turbine Technology and the Future of Wind Energy | AltEnergyMag.”

[3] Z. Ren, A. S. Verma, Y. Li, J. J. E. Teuwen, and Z. Jiang, “Offshore wind turbine operations and maintenance : A state-of-the-art review,” *Renewable and Sustainable Energy Reviews*, vol. 144, p. 110886, Jul. 2021. [Online]. Available : https://www.sciencedirect.com/science/article/pii/S1364032121001805

[4] B. Johnston, A. Foley, J. Doran, and T. Littler, “Levelised cost of energy, A challenge for offshore wind,” *Renewable Energy*, vol. 160, pp. 876–885, Nov. 2020. [Online]. Available : https://www.sciencedirect.com/science/article/pii/S0960148120309241

[5] A. G. Gonzalez-Rodriguez, “Review of offshore wind farm cost components,” *Energy for Sustainable Development*, vol. 37, pp. 10–19, Apr. 2017. [Online]. Available : https://www.sciencedirect.com/science/article/pii/S0973082616303647

[6] R. Taninoki, K. Abe, T. Sukegawa, D. Azuma, and M. Nishikawa, “Dynamic Cable System for Floating Offshore Wind Power Generation,” p. 6.

[7] E. Gulski, R. Jongen, A. Rakowska, and K. Siodla, “Offshore Wind Farms On-Site Submarine Cable Testing and Diagnosis with Damped AC,” *Energies*, vol. 12, no. 19, p. 3703, Jan. 2019, number : 19 Publisher : Multidisciplinary Digital Publishing Institute. [Online]. Available : https://www.mdpi.com/1996-1073/12/19/3703

[8] F. Dinmohammadi, D. Flynn, C. Bailey, M. Pecht, C. Yin, P. Rajaguru, and V. Robu, “Predicting Damage and Life Expectancy of Subsea Power Cables in Offshore Renewable Energy Applications,” *IEEE Access*, vol. 7, pp. 54 658–54 669, 2019, conference Name : IEEE Access.

[9] M. Marta, S. Mueller-Schuetze, H. Ottersberg, D. Isus, L. Johanning, and P. R. Thies, “Development of dynamic submarine MV power cable design solutions for floating offshore renewable energy applications,” Jun. 2015, accepted : 2015-09-24T11 :02 :59Z. [Online]. Available : https://ore.exeter.ac.uk/repository/handle/10871/18314

[10] P. R. Thies, L. Johanning, I. Bashir, T. Tuk, M. Tuk, M. Marta, and S. Müller-Schütze, “Accelerated reliability testing of articulated cable bend restrictor for offshore wind applications,” *International Journal of Marine Energy*, vol. 16, pp. 65–82, Dec. 2016. [Online]. Available : https://www.sciencedirect.com/science/article/pii/S2214166916300376

[11] A. Reda, J. Thiedeman, M. A. Elgazzar, M. A. Shahin, I. A. Sultan, and K. K. McKee, “Design of subsea cables/umbilicals for in-service abrasion - Part 1 : Case studies,” *Ocean Engineering*, p. 108895, May 2021.

[12] D. G. Young, C. Ng, S. Oterkus, Q. Li, and L. Johanning, “Assessing the mechanical stresses of dynamic cables for floating offshore wind applications,” *Journal of Physics : Conference Series*, vol. 1102, p. 012016, Oct. 2018, publisher : IOP Publishing. [Online]. Available : https://doi.org/10.1088/1742-6596/1102/1/012016

[13] B. Sonerud, F. Eggertsen, S. Nilsson, K. M. Furuheim, and G. Evenset, “Material considerations for submarine high voltage XLPE cables for dynamic applications,” in *2012 Annual Report Conference on Electrical Insulation and Dielectric Phenomena*, Oct. 2012, pp. 890–893, iSSN : 0084-9162.

[14] J. Densley, “Ageing mechanisms and diagnostics for power cables - an overview,” *IEEE Electrical Insulation Magazine*, vol. 17, no. 1, pp. 14–22, Jan. 2001, conference Name : IEEE Electrical Insulation Magazine.

[15] S. Emmanuel, M. Abdelghani, and S. Thomas, “A new time-domain model-based diagnosis method for assessing the offshore floating wind turbine umbilical state of health,” *Jcable*, p. 1, 2019.

[16] H. Suzuki and T. Endoh, “Pattern recognition of partial discharge in XLPE cables using a neural network,” *IEEE Transactions on Electrical Insulation*, vol. 27, no. 3, pp. 543–549, Jun. 1992, conference Name : IEEE Transactions on Electrical Insulation.

[17] B. Oyegoke, P. Hyvoenen, and M. Aro, “Partial discharge measurement as diagnostic tool for power cable systems. Literature review,” Jul. 2001. [Online]. Available : https://www.osti.gov/etdeweb/biblio/20226395

[18] Y. Xu, X. Gu, B. Liu, B. Hui, Z. Ren, and S. Meng, “Special requirements of high frequency current transformers in the on-line detection of partial discharges in power cables,” *IEEE Electrical Insulation Magazine*, vol. 32, no. 6, pp. 8–19, Nov. 2016, conference Name : IEEE Electrical Insulation Magazine.

[19] H. M. Lee, G. S. Lee, G.-Y. Kwon, S. S. Bang, and Y.-J. Shin, “Industrial Applications of Cable Diagnostics and Monitoring Cables via Time–Frequency Domain Reflectometry,” *IEEE Sensors Journal*, vol. 21, no. 2, pp. 1082–1091, Jan. 2021, conference Name : IEEE Sensors Journal.

[20] J. Wang, P. E. C. Stone, D. Coats, Y.-J. Shin, and R. A. Dougal, “Health Monitoring of Power Cable via Joint Time-Frequency Domain Reflectometry,” *IEEE Transactions on Instrumentation and Measurement*, vol. 60, no. 3, pp. 1047–1053, Mar. 2011, conference Name : IEEE Transactions on Instrumentation and Measurement.

[21] F. Böhme, R. Pietsch, U. Kaltenborn, and M. Hensel, “Cable Fault Location in High Voltage Cables – A New Solution,” in *2019 IEEE PES GTD Grand International Conference and Exposition Asia (GTD Asia)*, Mar. 2019, pp. 406–410.

[22] M. Bawart, M. Marzinotto, and G. Mazzanti, “Diagnosis and location of faults in submarine power cables,” *IEEE Electrical Insulation Magazine*, vol. 32, no. 4, pp. 24–37, Jul. 2016, conference Name : IEEE Electrical Insulation Magazine.

[23] C. M. Furse, M. Kafal, R. Razzaghi, and Y.-J. Shin, “Fault Diagnosis for Electrical Systems and Power Networks : A Review,” *IEEE Sensors Journal*, vol. 21, no. 2, pp. 888–906, Jan. 2021, conference Name : IEEE Sensors Journal.

[24] Q. Jiang and Q. Sui, “Technological study on distributed fiber sensor monitoring of high voltage power cable in seafloor,” in *2009 IEEE International Conference on Automation and Logistics*, Aug. 2009, pp. 1154–1157, iSSN : 2161-816X.

[25] V. Barinov, D. Kiesewetter, D. Shatilov, and A. Pyltzov, "Fiber optic temperature monitoring system of power cable lines," in *2017 10th International Symposium on Advanced Topics in Electrical Engineering (ATEE)*, Mar. 2017, pp. 641–644.

[26] R. Ross, "Inception and propagation mechanisms of water treeing," *IEEE Transactions on Dielectrics and Electrical Insulation*, vol. 5, no. 5, pp. 660–680, Oct. 1998, conference Name : IEEE Transactions on Dielectrics and Electrical Insulation.

[27] W. Reid, L. Rose, V. Rose, A. Campus, C. Baker, and J. Walton, "Water-tree degradation in power cable insulation : understanding and prevention," in *1992., Sixth International Conference on Dielectric Materials, Measurements and Applications*, Sep. 1992, pp. 496–499.

[28] K. Abdollal, "Water treeing as a function of moisture present in XLPE cable insulation," Jan. 1987. [Online]. Available : https://www.osti.gov/etdeweb/biblio/6069919

[29] S. Hvidsten, E. Ildstad, J. Sletbak, and H. Faremo, "Understanding water treeing mechanisms in the development of diagnostic test methods," *IEEE Transactions on Dielectrics and Electrical Insulation*, vol. 5, no. 5, pp. 754–760, Oct. 1998, conference Name : IEEE Transactions on Dielectrics and Electrical Insulation.

[30] W. Zhang, D. Yang, and H. Wang, "Data-Driven Methods for Predictive Maintenance of Industrial Equipment : A Survey," *IEEE Systems Journal*, vol. 13, no. 3, pp. 2213–2227, Sep. 2019, conference Name : IEEE Systems Journal.

[31] Z. Gao, C. Cecati, and S. X. Ding, "A Survey of Fault Diagnosis and Fault-Tolerant Techniques—Part I : Fault Diagnosis With Model-Based and Signal-Based Approaches," *IEEE Transactions on Industrial Electronics*, vol. 62, no. 6, pp. 3757–3767, Jun. 2015.

[32] E. Schaeffer, F. Auger, Z. Shi, P. Guillemet, and L. Loron, "Comparative Analysis of Some Parametric Model Structures Dedicated to EDLC Diagnosis," *IEEE Transactions on Industrial Electronics*, vol. 63, no. 1, pp. 387–396, Jan. 2016, conference Name : IEEE Transactions on Industrial Electronics.

[33] T. Söderström and P. Stoica, "Some properties of the output error method," *Automatica*, vol. 18, no. 1, pp. 93–99, Jan. 1982. [Online]. Available : https://www.sciencedirect.com/science/article/pii/0005109882900310

[34] J. Richalet, S. A. el Ata-Doss, and A. Coïc, "Global Identification and Optimal Input Design," *IFAC Proceedings Volumes*, vol. 24, no. 3, pp. 1121–1126, Jul. 1991. [Online]. Available : https://linkinghub.elsevier.com/retrieve/pii/S1474667017525008

[35] J.-C. Trigeassou, T. Poinot, and S. Bachir, "Parameter estimation for knowledge and diagnosis of electrical machines," in *Control Methods for Electrical Machines*, I. Ltd and J. W. . S. Inc, Eds. ISTE Ltd and John Wiley & Sons Inc, Jan. 2009, pp. 207–243. [Online]. Available : https://hal.archives-ouvertes.fr/hal-00782890

[36] Q. Nguyen-Duc, Y. L. Menach, S. Clenet, D. Vizireanu, and V. Costan, "Impedance Determination in Frequency Domain for Energy Cables by FEM and TLM," p. 9.

[37] S. Cristina and M. Feliziani, "A finite element technique for multiconductor cable parameters calculation," *IEEE Transactions on Magnetics*, vol. 25, no. 4, pp. 2986–2988, 1989.

[38] M. Shafieipour, Z. Chen, A. Menshov, J. De Silva, and V. Okhmatovski, "Efficiently computing the electrical parameters of cables with arbitrary cross-sections using the method-of-moments," *Electric Power Systems Research*, vol. 162, pp. 37 – 49, 2018. [Online]. Available : http://www.sciencedirect.com/science/article/pii/S0378779618301202